Supplemental Material for "Probing electron-phonon interactions away from the Fermi level with resonant inelastic x-ray scattering"

C. D. Dashwood,[1,*] A. Geondzhian,[2,3,†] J. G. Vale,[1] A. C. Pakpour-Tabrizi,[4] C. A. Howard,[1] Q. Faure,[1] L. S. I. Veiga,[1] D. Meyers,[5,6] S. G. Chiuzbăian,[7,8] A. Nicolaou,[7] N. Jaouen,[7] R. B. Jackman,[4] A. Nag,[9] M. García-Fernández,[9] Ke-Jin Zhou,[9] A. C. Walters,[9] K. Gilmore,[5,10,11] D. F. McMorrow,[1] and M. P. M. Dean[5,‡]

[1] *London Centre for Nanotechnology and Department of Physics and Astronomy, University College London, London, WC1E 6BT, UK*

[2] *Max Planck POSTECH/KOREA Research Initiative, 37673 Pohang, South Korea*

[3] *Max Planck Institute for the Structure and Dynamics of Matter, Luruper Chaussee 149, 22761 Hamburg, Germany*

[4] *London Centre for Nanotechnology and Department of Electronic and Electrical Engineering, University College London, London, WC1E 6BT, UK*

[5] *Condensed Matter Physics and Materials Science Department, Brookhaven National Laboratory, Upton, New York 11973, USA*

[6] *Department of Physics, Oklahoma State University, Stillwater, Oklahoma 74078, USA*

[7] *Synchrotron SOLEIL, L'Orme des Merisiers, Saint-Aubin, BP 48, 91192 Gif-sur-Yvette, France*

[8] *Sorbonne Université, CNRS, Laboratoire de Chimie Physique-Matiére et Rayonnement, UMR 7614, 4 place Jussieu, 75252 Paris Cedex 05, France*

[9] *Diamond Light Source, Didcot, Oxfordshire, OX11 0DE, UK*

[10] *Physics Department and IRIS Adlershof, Humboldt-Universität zu Berlin, Zum Großen Windkanal 2, 12489 Berlin, Germany*

[11] *European Theoretical Spectroscopy Facility (ETSF)*

I. SELF-ABSORPTION CORRECTION

Self-absorption – the re-absorption by the sample of previously scattered photons – depends on the energies and angles of both the incident and outgoing x-rays, and must therefore be corrected to reliably compare spectra. We follow previous resonant inelastic x-ray scattering (RIXS) studies [1–3] and define a self-absorption correction factor

$$C_{\boldsymbol{\epsilon},\boldsymbol{\epsilon}'}(2\Theta,\theta,\omega_i,\omega_o) = \frac{1}{1+u(2\Theta,\theta)t_{\boldsymbol{\epsilon},\boldsymbol{\epsilon}'}(\omega_i,\omega_o)}. \tag{1}$$

In this expression, $u = \sin\theta/\sin(2\Theta-\theta)$ is a geometrical term that depends on the scattering angle $2\Theta = 154°$, and sample angle $\theta = 20°$ $(90°)$ for the π^* (σ^*) spectra. The other term

$$t_{\boldsymbol{\epsilon},\boldsymbol{\epsilon}'}(\omega_i,\omega_o) = \frac{\alpha_0+\alpha_{\boldsymbol{\epsilon}}(\omega_i)}{\alpha_0+\alpha_{\boldsymbol{\epsilon}'}(\omega_o)} \tag{2}$$

depends on α_0, the absorption coefficient before the resonance (taken at 284 eV for the π^* resonance and 289 eV for the σ^* resonance), and $\alpha_{\boldsymbol{\epsilon}}(\omega)$, the resonant absorption coefficient for x-rays with energy ω and polarization $\boldsymbol{\epsilon}$.

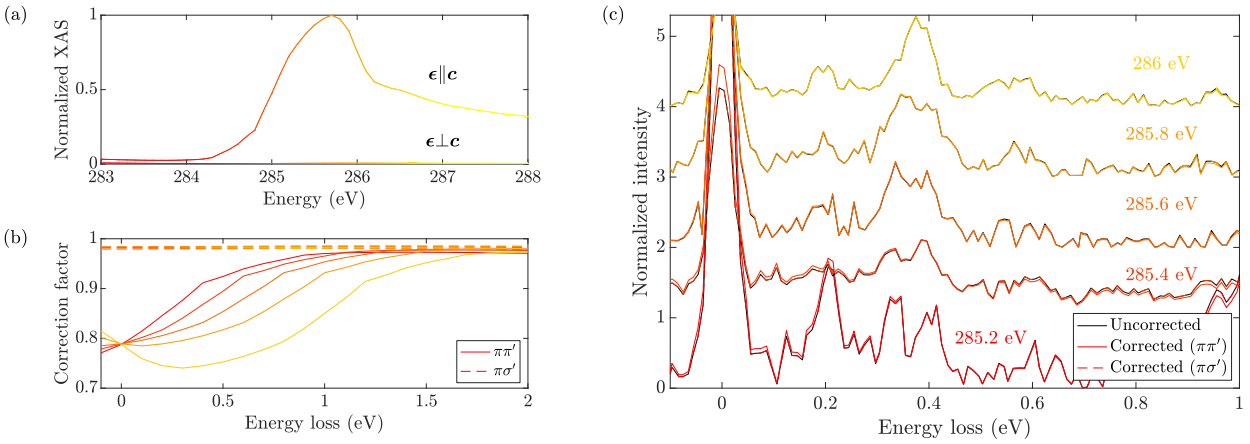

FIG. S1. (a) XAS around the π^* resonance with incident x-rays polarized parallel ($\boldsymbol{\epsilon}\|\boldsymbol{c}$) and perpendicular ($\boldsymbol{\epsilon}\perp\boldsymbol{c}$) to the $\boldsymbol{c}$ axis. (b) Self-absorption correction factors in the $\pi\pi'$ (solid) and $\pi\sigma'$ (dashed) polarization channels, with colours corresponding to the incident energies labelled in (c). (c) Uncorrected (black) and corrected (red to yellow) RIXS spectra in the two polarization channels, normalized to the intensity of the two-phonon peak. The corrections introduce changes below the noise level to the normalized spectra.

* cameron.dashwood.17@ucl.ac.uk; These authors contributed equally

† These authors contributed equally

‡ mdean@bnl.gov

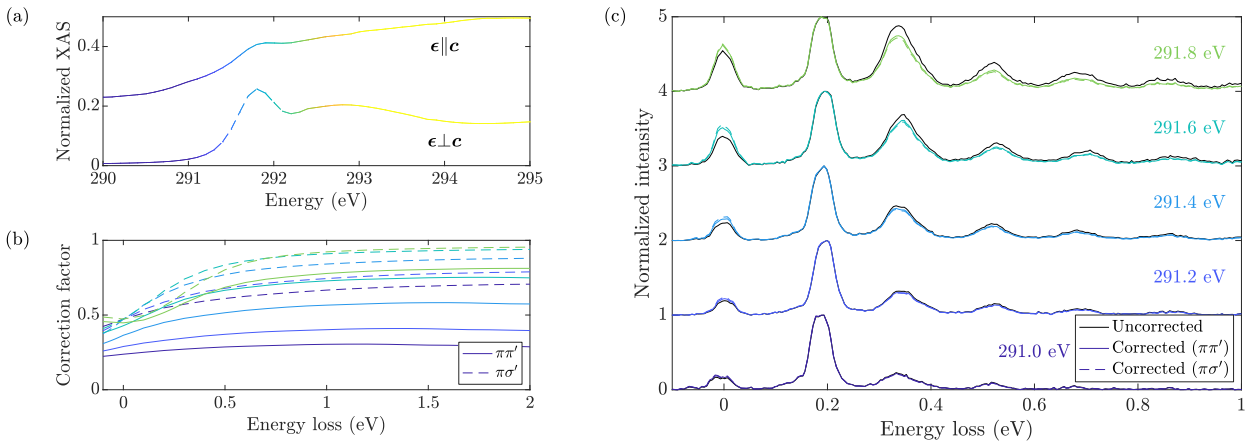

FIG. S2. (a) XAS around the σ^* resonance with incident x-rays polarized parallel ($\boldsymbol{\epsilon} \| \boldsymbol{c}$) and perpendicular ($\boldsymbol{\epsilon} \perp \boldsymbol{c}$) to the $\boldsymbol{c}$ axis. In this work we focus on the σ^{*1} resonance at 291.8 eV and ignore the broad σ^{*2} resonance above which arises from zero-point vibrations. (b) Self-absorption correction factors in the $\pi\pi'$ (solid) and $\pi\sigma'$ (dashed) polarization channels, with colours corresponding to the incident energies labelled in (c). (c) Uncorrected (black) and corrected (blue to green) RIXS spectra in the two polarization channels, normalized to the intensity of the one-phonon peak.

The absorption coefficients can be obtained from XAS measured in total electron yield, shown in Fig. S1(a) and S2(a). With our incident x-rays polarized in the $(h, 0, l)$ scattering plane (π polarization), we measure the absorption for $\boldsymbol{\epsilon} \| \boldsymbol{c}$ ($\boldsymbol{\epsilon} \perp \boldsymbol{c}$) using x-rays incident normal (grazing) to the sample surface. From these, we calculate the absorption coefficients as

$$\begin{aligned}
\alpha_\pi(\omega_i) &= \mathrm{XAS}(\omega_i, \boldsymbol{\epsilon} \perp \boldsymbol{c}) \sin^2\theta + \mathrm{XAS}(\omega_i, \boldsymbol{\epsilon} \| \boldsymbol{c}) \cos^2\theta, \\
\alpha_\pi(\omega_o) &= \mathrm{XAS}(\omega_o, \boldsymbol{\epsilon} \perp \boldsymbol{c}) \sin^2(2\Theta - \theta) + \mathrm{XAS}(\omega_o, \boldsymbol{\epsilon} \| \boldsymbol{c}) \cos^2(2\Theta - \theta), \\
\alpha_\sigma(\omega_o) &= \mathrm{XAS}(\omega_o, \boldsymbol{\epsilon} \perp \boldsymbol{c}).
\end{aligned} \tag{3}$$

The resulting correction factors are shown in Fig. S1(b) and S2(b). The RIXS spectra are then corrected by dividing through by $C_{\boldsymbol{\epsilon},\boldsymbol{\epsilon}'}(2\Theta, \theta, \omega_i, \omega_o)$.

The anisotropic absorption of graphite results in a significant polarization dependence of the correction factors, especially around the π^* resonance. The polarization of the outgoing photons will depend on the symmetry of the phonon modes being excited, and was not determined in our experiment. As our model only predicts the relative intensities of the phonon peaks, however, we can normalize the spectra to the intensity of the strongest

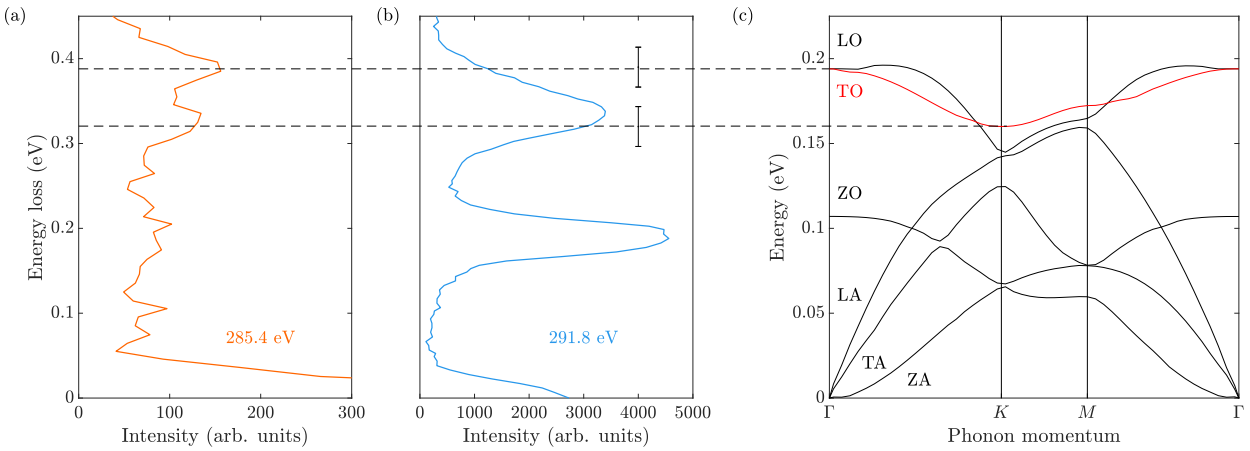

FIG. S3. Experimental RIXS spectra at (a) 285.4 eV and (b) 291.8 eV, alongside (c) the phonon dispersion of graphite from Ref. [4] scaled to half the energy range of (a) and (b). The horizontal dashed lines mark (twice) the energies of the TO mode at Γ and K, and the vertical error bars show the instrumental energy resolution.

multi-phonon peak. As shown in Fig. S1(c) and S2(c), after normalisation the difference between the corrected spectra is minimal over the energy range of interest, and does not significantly affect the fits to our model. We therefore correct all spectra assuming that the outgoing photons are π polarised.

II. ASSIGNMENT OF PHONON MODES

In the main text, we assign the contributions to the RIXS spectra based on the known phonon dispersion of graphite [4]. Here we demonstrate this process for the two-phonon features. Fig. S3 shows spectra near the π^* and σ^* resonances plotted alongside the phonon dispersion, scaled such that the phonon energies line up with twice the energy loss of the spectra. From this, it is clear that the two peaks in the split feature of the π^* spectrum occur at twice the energies of transverse optical (TO) phonons at Γ and K, while the broad asymmetric feature of the σ^* spectrum spans twice the bandwidth of the TO mode. Taking into account the 47 meV experimental energy resolution, it can be seen that contributions from the acoustic (ZA, TA, and LA) and out-of-plane optical (ZO) modes are negligible, and the longitudinal optical (LO) mode could only have significant contributions when it is nearly degenerate with the TO mode.

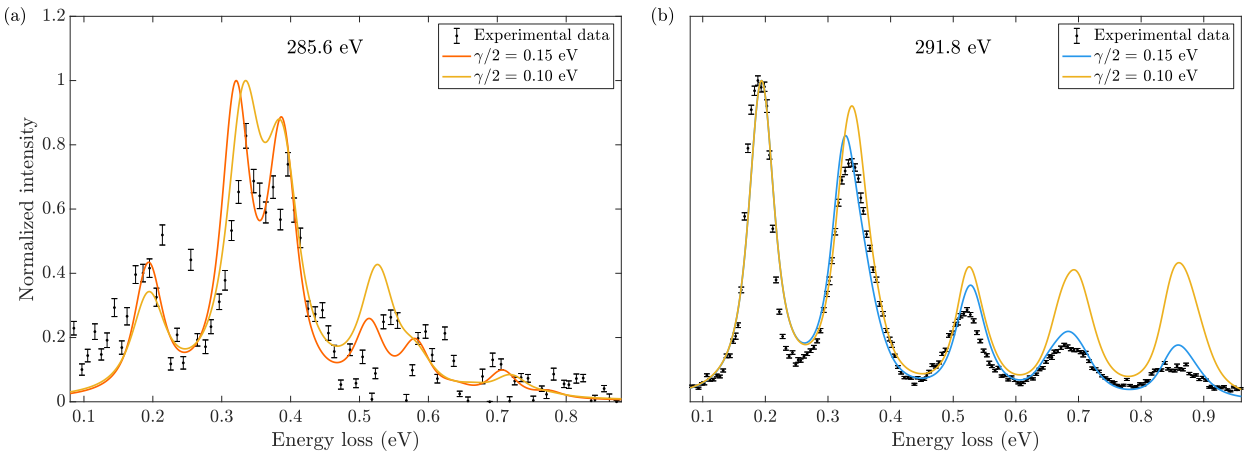

FIG. S4. Comparison of best-fit RIXS spectra at (a) the π^* and (b) the σ^* resonance with half inverse intermediate-state lifetimes of $\gamma/2 = 0.15\,\text{eV}$ (orange/blue) and $0.10\,\text{eV}$ (yellow).

III. INTERMEDIATE-STATE LIFETIME

To model our RIXS spectra we adjusted the intermediate-state lifetime from the value $\gamma/2 = 0.1\,\text{eV}$ (half-width at half-maximum of the Lorentzian component of the spectral peak) measured by x-ray photoemission spectroscopy [5] due to the presence of the extra excited electron in RIXS. Figure S4 compares best-fit RIXS spectra at the π^* and σ^* resonances calculated using the bare core-hole lifetime $0.1\,\text{eV}$, to the adjusted value $0.15\,\text{eV}$. We can see that the adjusted lifetime gives better agreement with both experimental spectra, especially for the high-order peaks at the σ^* resonance. This adjusted lifetime was used for all calculations shown in the main manuscript, successfully reproducing the energy dependence of the experimental spectra below both resonances.

IV. INDEPENDENT FITTING OF THE ENERGY-DEPENDENT SPECTRA

The calculated spectra shown in Fig. 3(c) of the main manuscript are the result of a simultaneous fit to the experimental spectra around the π^* resonance, such that the only parameter of the model that is varied between the spectra is the incident energy.

We have also fitted the spectra at each energy independently to see how this affects the extracted electron-phonon (e-ph) interaction strengths. Figure S5 shows a comparison of the simultaneous and independent fits, with the resulting values of $G(\boldsymbol{q})$ listed in Table S1. Both sets of calculated spectra have an acceptable level of agreement with the experimental

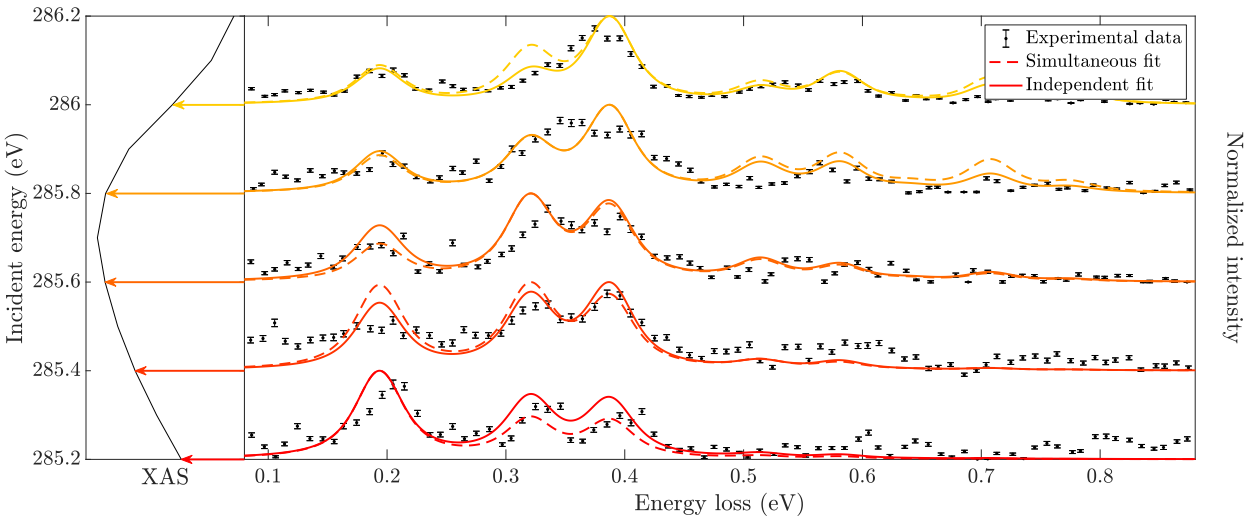

FIG. S5. Comparison of independent (solid colored lines) and simultaneous (dashed coloured lines) fits to the experimental RIXS spectra (black points with error bars) around the π^* resonance, plotted alongside the XAS with arrows indicating the energies.

TABLE S1. $G(\boldsymbol{q})$ extracted from simultaneous and independent fits to the RIXS spectra around the π^* resonance, at the momenta Γ, $\boldsymbol{q}_{\text{exp}} \approx (0.08, 0.00)$, $K - \boldsymbol{q}_{\text{exp}}$, and K.

G (eV)	$\boldsymbol{q} = \Gamma$	$\boldsymbol{q} = \boldsymbol{q}_{\text{exp}}$	$\boldsymbol{q} = K - \boldsymbol{q}_{\text{exp}}$	$\boldsymbol{q} = K$
Simultaneous fit	0.23	0.05	0.06	0.32
$\hbar\omega_i = 285.2\,\text{eV}$	0.24	0.05	0.13	0.30
$\hbar\omega_i = 285.4\,\text{eV}$	0.24	0.05	0.07	0.30
$\hbar\omega_i = 285.6\,\text{eV}$	0.23	0.07	0.07	0.32
$\hbar\omega_i = 285.8\,\text{eV}$	0.20	0.05	0.05	0.28
$\hbar\omega_i = 286.0\,\text{eV}$	0.24	0.05	0.12	0.27

data given the noise level, but the independent fits do offer better agreement especially for the spectrum at 286 eV. As we note in the main text, we expect composition of the intermediate electronic state and therefore the momentum dependence of G to vary in the high-energy tail of the XAS peak, providing a natural explanation for this. While Table S1 shows some variation in the extracted interaction strengths, the general trend of $G(\boldsymbol{q})$ through the Brillouin zone – with $G(K) > G(\Gamma) >> G(K - \boldsymbol{q}_{\text{exp}}) \geq G(\boldsymbol{q}_{\text{exp}})$ – is valid irrespective of the fitting procedure.

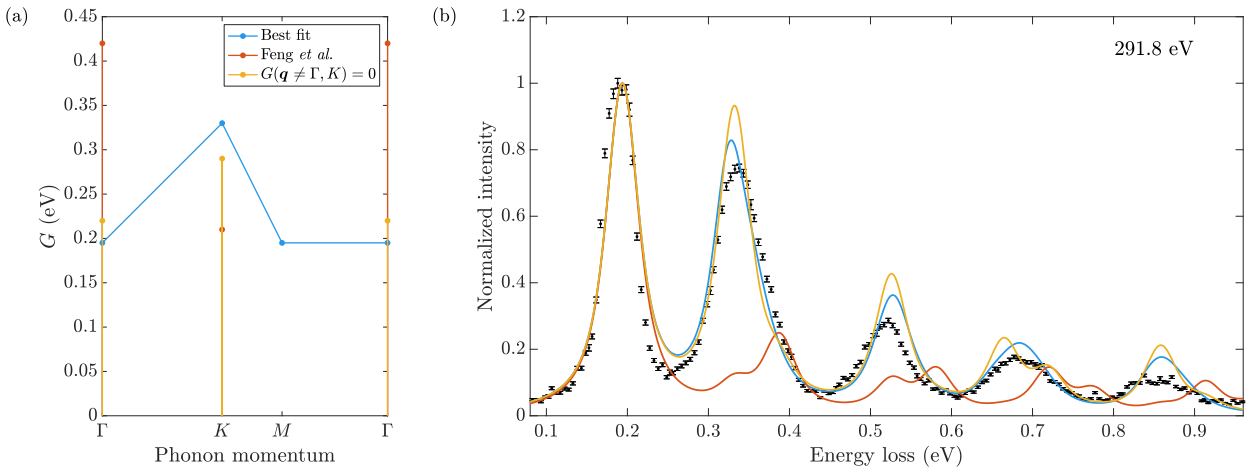

FIG. S6. (a) Our best-fit $G(\boldsymbol{q})$ for σ^* electrons (blue), compared to that obtained by Feng *et al.* [3] (orange) and our best-fit with G constrained to be finite only at $\boldsymbol{q} = \Gamma$ and K (yellow). (b) Comparison of calculated RIXS spectra at the σ^* resonance, with colours corresponding to those in (a) and the experimental spectrum shown as black points with error bars. All spectra are calculated with an intermediate-state lifetime $\gamma/2 = 0.15\,\text{eV}$.

V. COMPARISON WITH PREVIOUS RIXS MEASUREMENTS ON GRAPHITE

Feng *et al.* recently presented lower-resolution RIXS measurements around the σ^* resonance of graphite [3], interpreting their data with reference to Raman spectroscopy results. Their analysis implicitly assumed, however, a coupling of phonons to electrons near the Fermi level, leading them to constrain $G(\boldsymbol{q})$ to be non-zero only at the Γ and K points. While this is reasonably accurate for the π^* resonance, we show in the main text that RIXS at the σ^* resonance probes the interaction of phonons with elections *away* from the Fermi level, whose strength is significant throughout the Brillouin zone. As well as overlooking the possibilities afforded by tuning the incident photon energy, this serves as a warning that careful consideration of the states involved in the RIXS process is essential for correct interpretation of experimental spectra, especially if the energy resolution is lacking.

We compare our best-fit $G(\boldsymbol{q})$ at the σ^* resonance (blue), to that obtained by Feng *et al.* (orange) in Fig. S6(a). From the resulting normalized spectra in Fig. S6(b), we see that the couplings from Feng *et al.* give a poor fit to all of the multi-phonon peaks.

We can also investigate the effect of phonon mode mixing in the intermediate RIXS state through a direct comparison to the results of Feng *et al.*, who neglect it in their

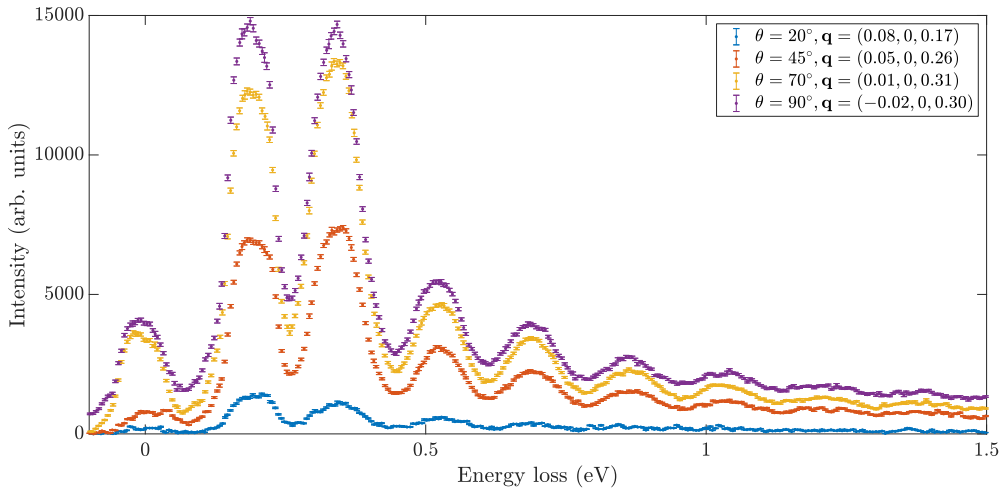

FIG. S7. Momentum dependence along $(h, 0, l)$ of the experimental RIXS spectra at the σ^* resonance.

modeling. Even if the final RIXS state consists of only a single phonon, the intermediate state can contain many modes which non-linearly affect the cross-section [6]. Let us briefly set aside what we know about the momentum dependence of G away from the Fermi level, and fit our σ^* spectrum with contributions from only Γ and K (yellow in Fig. S6). While the calculated spectrum does not agree with the experimental data as well as our best fit, especially in the high-order peaks which become split, we see that the values of M_Γ and M_K approach those of our linearly-varying model. Our model yields a ratio $G(\Gamma)/G(K) = 0.79$, compared to $G(\Gamma)/G(K) = 2.1$ obtained by Feng *et al.* (note that $G(\Gamma)/G(K)$ is insensitive to the different intermediate-state lifetimes used, as in the Ament model the relative peak intensities depend on the ratio of G to lifetime). We therefore see that, even for the relatively flat optical modes studied here, accounting for intermediate-state mixing strongly affects the momentum-dependence of G extracted from the data.

VI. MOMENTUM DEPENDENCE OF THE RIXS SPECTRA

The maximum momentum transfer is limited by the low energy of the carbon K edge. Additionally, the RIXS cross-section falls off rapidly for sample angles away from $\theta = 0°$ (grazing incidence) at the π^* resonance, and away from $\theta = 90°$ (normal incidence) at the σ^* resonance. In the main manuscript, we show how these restrictions can be circumvented by analysing the contributions to the multi-phonon peaks, which can come from phonons

throughout the Brillouin zone.

Figure S7 shows the momentum-dependence of the RIXS spectra at the σ^* resonance along the $(h, 0, l)$ direction. The in-plane momentum was varied by changing the sample angle θ while keeping the spectrometer angle $2\Theta(\neq 2 \times \theta)$ fixed, so the total momentum transfer $q \propto \sqrt{4h^2/(3a^2) + l^2/c^2}$ is constant. While the overall intensity falls off rapidly with decreasing θ, it can be seen that the relative intensities of the phonon peaks change only minimally, supporting our conclusion that $G(\boldsymbol{q})$ varies gradually away from the Γ point.

The low intensity of the phonon features at the π^* resonance, along with the strong fall-off in intensity with increasing θ, precluded measurement of a momentum-dependence with reasonable statistics.

---

[1] M. Rossi, R. Arpaia, R. Fumagalli, M. Moretti Sala, D. Betto, K. Kummer, G. M. De Luca, J. van den Brink, M. Salluzzo, N. B. Brookes, L. Braicovich, and G. Ghiringhelli, Experimental determination of momentum-resolved electron-phonon coupling, Phys. Rev. Lett. **123**, 027001 (2019).

[2] J. G. Vale, C. D. Dashwood, E. Paris, L. S. Veiga, M. Garcia-Fernandez, A. Nag, A. Walters, K. J. Zhou, I. M. Pietsch, A. Jesche, P. Gegenwart, R. Coldea, T. Schmitt, and D. F. Mcmorrow, High-resolution resonant inelastic x-ray scattering study of the electron-phonon coupling in honeycomb $\alpha - Li_2IrO_3$, Phys. Rev. B **100**, 224303 (2019).

[3] X. Feng, S. Sallis, Y.-C. Shao, R. Qiao, Y.-S. Liu, L. C. Kao, A. S. Tremsin, Z. Hussain, W. Yang, J. Guo, and Y.-D. Chuang, Disparate exciton-phonon couplings for zone-center and boundary phonons in solid-state graphite, Phys. Rev. Lett. **125**, 116401 (2020).

[4] M. Mohr, J. Maultzsch, E. Dobardžić, S. Reich, I. Milošević, M. Damnjanović, A. Bosak, M. Krisch, and C. Thomsen, Phonon dispersion of graphite by inelastic x-ray scattering, Phys. Rev. B **76**, 035439 (2007).

[5] F. Sette, G. K. Wertheim, Y. Ma, G. Meigs, S. Modesti, and C. T. Chen, Lifetime and screening of the C $1s$ photoemission in graphite, Phys. Rev. B **41**, 9766 (1990).

[6] A. Geondzhian and K. Gilmore, Generalization of the Franck-Condon model for phonon excitations by resonant inelastic x-ray scattering, Phys. Rev. B **101**, 214307 (2020).